

# ANALYSIS OF LAND SKIN TEMPERATURE USING AVHRR OBSERVATIONS

BY MENGLIN JIN

This newly developed 18-yr AVHRR-based dataset can show the diurnal, seasonal, and interannual variations of land surface skin temperatures.

Satellite-based surface temperature is referred to as skin temperature (Dickinson 1994). The National Research Council (NRC; 2000) and the Intergovernmental Panel on Climate Change (IPCC; Houghton et al. 2001) pointed out the urgent need for long-term remote sensing-based land surface skin temperature (LST) data in global warming studies to improve the limits of conventional 2-m World Meteorological Organization (WMO) surface air temperature observations ( $T_a$ ). Currently, the long-term surface skin temperature dataset is only available over the ocean [i.e., sea surface temperature (SST), Bates and Diaz 1991]. Over land, developing such a dataset has proved more difficult due to the land's high surface heterogeneities.

Beside being an indicator of climate change, skin temperature (in particular, its diurnal cycle) is needed in calculating sensible and latent heat fluxes. Specifically, sensible heat flux is determined by the instantaneous difference between LST and near-surface  $T_a$ . In the conventional bulk equation, the use of daily averaged LST instead of hourly LST can result in errors up to  $100 \text{ W m}^{-2}$ .

The National Oceanic and Atmospheric Administration (NOAA) polar-orbiting satellites have unique advantages for the LST dataset development because of a long observation period, global coverage, easy data access, an abundance of excellent research, and operational efforts to promote a retrieval process of the highest quality possible. NOAA's Advanced Very High Resolution Radiometer (AVHRR) uses thermal infrared channels to measure the radiative emission of the surface. LST can be derived from AVHRR radiances after removing atmospheric and surface emissivity effects (Ulivieri et al. 1994; Wan and Dozier 1996; Becker and Li 1995; Prata et al. 1995; Kerr 1997). However, AVHRR radiance is measured only twice per day for most areas. How to interpolate these twice-per-day observations into diurnal cycles has been studied for years and is still an ongoing research topic (Jin and Dickinson 1999, 2000;

**AFFILIATIONS:** JIN—Department of Meteorology, University of Maryland, College Park, College Park, Maryland

**CORRESPONDING AUTHOR:** Dr. Menglin Jin, Department of Meteorology, University of Maryland, College Park, College Park, MD 20742

E-mail: [mjin@atmos.umd.edu](mailto:mjin@atmos.umd.edu)

DOI: 10.1175/BAMS-85-4-587

In final form 21 October 2003

©2004 American Meteorological Society

Jin 2000). Furthermore, significant orbital drift in the afternoon paths of NOAA-7, -9, -11, and -14 hinders LSTD development (see Fig. 1) because such drift makes AVHRR skin temperature data temporally inhomogeneous. In addition, at thermal infrared wavelengths, cloud contamination precludes the satellite from measuring surface skin temperature.

To correct the above-mentioned problems, we have developed algorithms as described by serial papers, which are outlined in the next section (Jin and Dickinson 1999, 2000; Jin 2000; Jin and Treadon 2003). Based on monthly AVHRR LST and these algorithms, we have developed a diurnal cycle dataset, namely LSTD. LSTD contains monthly mean global 8-km resolution data from 1981 to 1998. Great effort has also been made to develop a physically meaningful scale-up method to average the 8-km LSTD into a model grid scale on the order of 100 km.

Validating LSTD is important and challenging. We used two methods to validate LSTD: one is to intercompare LSTD with other LST observations, and another is to use LSTD in climate studies and compare the results with our existing understanding. As proven in many other cases, the latter is a practical approach for validating the new dataset. In this paper, we present diurnal, seasonal, and interannual variations of LST. In the remaining part of this paper, section 2 outlines the difficulties in LSTD developments and our approaches. Section 3 shows data,

while section 4 highlights prototype examples of how to use LSTD in climate study and presents some validation results. Furthermore, brief concluding remarks are given in section 5 to discuss the strengths and limits of LSTD and future directions of this work.

**DIFFICULTIES AND APPROACHES.** Conventional WMO 2-m  $T_a$  is a thermodynamically defined quantity. LST, however, is radiative temperature measured by a radiometer mounted above the surface. LST is different from the WMO  $T_a$  temperature in both physical meaning and magnitude, but is closely related to the latter (Norman and Becker 1995). LST depends on the infrared wavelength used for the measurement, spectral dependence of the emissivity, angle at which the measurement is made, state of the surface (roughness, surface type, moisture, vegetation cover, etc.), and height of the instrument above the surface. Furthermore, the state of the atmosphere above (i.e., atmospheric moisture distribution, amount, and geometrical distribution of cloud cover and aerosol) also affects the accuracy of LST measurement. Consequently, a wide range of errors may occur when one tries to measure a single accurate LST measurement from space.

The major problems that prevent NOAA AVHRR from being used to develop a long-term LSTD include orbit drift, uncertainties in skin temperature retrieval (such as that induced by unknown surface emissivity), unknown cloud occurrence during a day other than at observing time, lack of LST diurnal cycle measurement, and/or volcanic eruption. Below we discuss these problems and our current approaches in turn.

*Orbit drift.* AVHRR skin temperature measurements cannot be directly used in climate change studies because of orbit drift in the NOAA satellites (particularly, NOAA-7, -9, -11, and -14) over the course of these satellites' lifetimes (Price 1991; Ignatov and Gutman 1999; Hurrell and Trenberth 1992; Susskind 2001, personal communication; Jin and Treadon 2003). Figure 1 schematically illustrates the change in the NOAA satellites' northbound equatorial crossing time due to orbit drift. For example, NOAA-11 initially observed the surface around 1330 local time (LT) in 1989 but, by the end of 1994, its overpass time shifted to 1700 LT. This drift is attributable to the original design meant to keep satellite instruments out of direct sunlight (Price 1991). Jin and Treadon (2003) shows that the orbit drift of the NOAA-7, -9, -11, and -14 series of satellites results in a significant cooling effect on LST measurements. This effect is combined with the signal of the true variations in the climate system and,

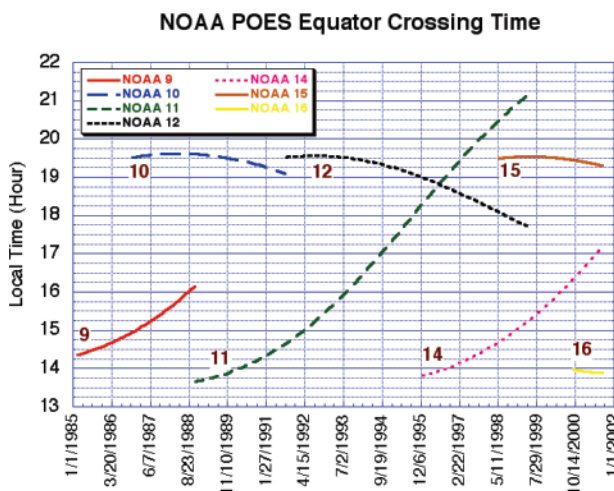


**FIG. 1. Schematic diagram of the equatorial crossing time for NOAA-9, -10, -11, -12, -14, -15, and -16. The y direction is local equatorial crossing time, and the x direction is time of year. NOAA-7 is not shown here, but has a similar orbital drift as the afternoon satellites of NOAA-9, -11, and -14. (This figure is provided by H. T. Lee of Department of Meteorology, University of Maryland.)**

thus, makes the observed LST temporally inconsistent. Applying a physically-based “typical pattern technique” to remove the orbit drift effect from LST, Jin and Treadon (2003) utilized a lookup table of typical land skin temperature diurnal cycles derived from the National Center for Atmospheric Research (NCAR) Climate Community Model (CCM) 3 coupled with the land surface model, Biosphere–Atmosphere Transfer Scheme (BATS). The GCM-generated typical patterns of the LST diurnal cycle are functions of vegetation type, season, and latitude, and are combined with satellite observations to remove the cooling effect. Applying this methodology to 18 yr of AVHRR (1981–98) LST observations evidently yields an improved skin temperature dataset suitable for climate change study (Jin and Dickinson 2002).

*Emissivity in skin temperature retrieval.* Remotely sensed surface temperature is retrieved from thermal emission measured at various wavelengths at which the atmosphere is relatively transparent, that is, in the “window” region. However, even in the most transparent spectral windows for clear skies, atmospheric emission and attenuation are not negligible. Thus, corrections for atmospheric effects are usually required.

The split-window technique (SWT) is the most widely used correction technique for AVHRR skin temperature retrieval. First proposed in 1970 for SST retrieval, SWT assumes that atmospheric absorption can be approximated as a linear combination of the radiances measured at two different wavelengths (Sobrino et al. 1994). This technique was applied to the land surface with success (Price 1984; Cooper and Asrar 1989; Becker and Li 1990; Parata et al. 1995; Wan and Dozier 1996). Originated from the spectral transfer equation, SWT is usually written in “classical” form as suggested by Prabhakara et al. (1974, after Stephens 1994):

$$\text{LST} \approx T_{b,1} + \xi(T_{b,1} - T_{b,2}), \quad (1)$$

where  $T_{b,1}$  and  $T_{b,2}$  are brightness measurements at two thermal number channels, and  $\xi$  is the function of optical depth in the two channels. A more typical form of the split-window method in remote sensing is

$$\text{LST} = aT_1 + b(T_1 - T_2) - c, \quad (2)$$

which was initially presented in Price (1984), where  $a$ ,  $b$ , and  $c$  in this equation are either constants or functions of surface emissivity.

SWT requires knowledge of accurate land surface emissivity. However, emissivity is difficult to measure

because, in the real world, it varies with surface vegetation density, soil chemical components, and soil physical conditions such as grain size, as well as view angle. Unlike the sea surface, where the emissivity at the wavelength of AVHRR channels 4 and 5 is high and well known, land surface emissivity is highly heterogeneous. As a result, emissivity is one of the largest uncertainty sources in SWT. The currently used approach is to set two emissivities for channels 4 and 5, respectively, and assume they do not vary over the globe. Obviously, such an approach is unrealistic and induces errors in LST retrieval.

*Approach to reduce emissivity uncertainty.* In LSTD, as a first-order approximation, we used Moderate Resolution Imaging Spectroradiometer (MODIS)-based emissivity information in SWT. Land surface emissivities have been retrieved at 5-km grids from pairs of day-and-night MODIS observations in seven thermal infrared bands with the physics-based day–night method (Wan and Li 1997). The MODIS LST product MOD11B1 provides emissivities in bands 20, 22, 23, 29, and 31–32, from which broadband emissivity can be inferred (Jin and Liang 2003, manuscript submitted to J. Climate, hereafter JL03). Evidently, Fig. 2 shows that emissivity has obvious variations over the globe, because it is a function of soil and vegetation conditions. In general, emissivity is approximately 0.95–0.97 for vegetated areas and 0.8–0.95 for most of the bare soil areas. In addition, evident seasonality is observed at emissivity fields (JL03).

Utilizing MODIS-based emissivity in the LSTD process is much more realistic than simply assuming two fixed spectral emissivities for AVHRR channels 4 and 5 over the globe, a treatment that is generally used in AVHRR LST retrieval due to the lack of emissivity measurements. Nevertheless, some uncertainties still remain. One is that emissivity is a function, moderately, of soil moisture. During the 1981–98 period, one given area may have experienced different rainfall patterns (drought or dry), which resulted in an emissivity departing from the MODIS-based typical values. In addition, some areas experienced land cover and land use changes that made the surface emissivity dramatically different (JL03). However, our research showed that emissivity made skin temperature different for each pixel, about 0.7°C per 1% emissivity uncertainty, which is consistent with the results of Prata et al. (1995). Yet the global annual anomaly for LST, which is of most concern in global change studies, did not get affected much, probably due to the emissivity-induced skin temperature variations compensating each other in the glo-

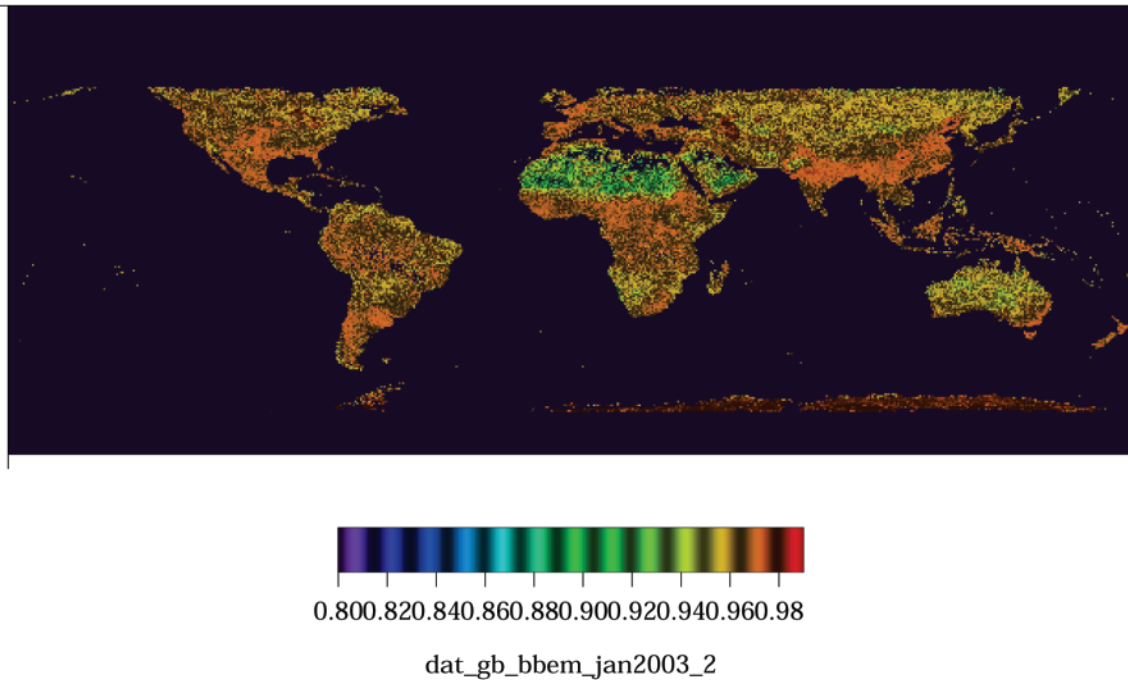


**FIG. 2. Global distribution of MODIS-observed land surface emissivity. It is broadband emissivity converted from MODIS spectral emissivity using MODTRAN (JL03). Data for oceans, Antarctica, and some equatorial deserts that are lower than 0.8 are missing values.**

bal average sense. Furthermore, a relatively small portion of land surface has experienced dramatic land cover and land use changes; therefore, when averaged over the globe, land cover-induced emissivity uncertainty can be ignored.

A simple mathematical analysis may help interpret this point. In our work, we used Ulivieri et al.'s (1994) split-window algorithm,

$$LST = a_0 T_4 + b_0 (T_4 - T_5) - \Delta \epsilon c_0 + d_0 (1 - \bar{\epsilon}), \quad (3)$$

where  $a_0$ ,  $b_0$ ,  $c_0$ , and  $d_0$  are constants with  $c_0 = 75$  and  $d_0 = 48$ . Respectively,  $T_4$  and  $T_5$  are the brightness temperatures of channels 4 and 5, while  $\Delta \epsilon$  is the difference between channel-4 and channel-5 spectral emissivities. The average of these two emissivities is represented by  $\bar{\epsilon}$ .

Then,

$$\frac{\partial LST}{\partial \Delta \epsilon} = -c_0, \quad (4)$$

$$\frac{\partial LST}{\partial \bar{\epsilon}} = -d_0. \quad (5)$$

Because emissivity uncertainty is approximately 0.5% for vegetation and 1% for bare soil (Kerr et al. 1997;

Wan and Dozier 1996), 1% inaccuracy of  $\Delta \epsilon$  and  $\bar{\epsilon}$  may cause a 0.5°–1.5°C error in LST. Generally, this accuracy is comparable with that of surface air temperature observations or GCM-simulated LST (Jin et al. 1997).

However, it is important to note that the coefficients in Eq. (3) shall depend on the spectral functions of channels 4 and 5, which may change with the series of NOAA satellites. The constants  $c_0$  and  $d_0$  are examples given by Ulivieri et al. (1994). Also keep in mind that Eq. (3) does not include important terms, that is,  $\Delta \epsilon \times (T_4 + T_5)$  and  $\Delta \epsilon \times (T_4 - T_5)$ . Therefore, the effects of the uncertainty in  $\Delta \epsilon$  should be very large, see Becker and Li (1990) and Wan and Dozier (1996, their Fig. 5).

**Cloud contamination.** Cloud contamination causes two problems in LSTD: an inability to directly measure LST when the surface is obscured by clouds, that is, the “cloudy pixel problem,” and the appearance of cloud formation during the day at times other than when the measurements were made.

Methods of calculating LST for a satellite cloudy pixel were designed in Jin (2000) and Jin and Dickinson (2000). The cloudy pixel treatment used is a hybrid technique of “neighboring pixel” and “surface air temperature” techniques. The principle of cloudy pixel treatment is based on the surface energy balance to infer a cloudy pixel’s LST from the neigh-

boring clear pixel's LST and overlying  $T_a$ . Soil heat flux is treated by a conventional force–restore method for bare soil or short vegetated surfaces, where ground heat flux is important. For other surfaces where soil heat flux is less important, heat flux is treated using the Bowen ratio method. This method is generalized into other surfaces in Jin and Dickinson (2000). Please refer to those two papers for details.

**Lack of diurnal cycle.** In general, polar-orbiting satellites observe a given pixel twice per day. They overpass high latitudes more frequently, but land areas over those areas are relatively small. Therefore, for most land surfaces, available LST observations are also available twice per day. In order to interpolate AVHRR twice-per-day LST into a diurnal cycle, we have developed a “typical pattern technique” as described in Jin and Dickinson (1999). In this approach, the climatological diurnal cycles of LST are derived from the most advanced model, NCAR CCM3 BATS, which served as the information base for the most likely behavior of diurnal cycle. Typical LST patterns are functions of land cover, latitude, season, and soil moisture conditions, and are archived in lookup tables. Given the geophysical location and land cover information for one given pixel after the AVHRR LST is measured, a typical pattern is extracted from the corresponding lookup table. Various methods are examined to fit the AVHRR LST into typical diurnal cycle patterns and to pass the prescribed quality control. The underlying physical foundation of the typical pattern technique is that the diurnal cycle of temperature can be viewed as a composite of a daily average, diurnal periodic component, and random aperiodic component (noise). With the assumption that the noise can be ignored, the daily average can be inferred from twice-per-day satellite measurements; the periodic part can be obtained from modeled climatologies, providing a practical approach for estimation of the diurnal cycle of skin temperature. The details of the typical pattern technique and its applications and validations can be found in Jin and Dickinson (1999) and Jin and Treadon (2003). The accuracy of this scheme is estimated to be about 1–1.5 K (see Jin and Dickinson 1999).

**Volcano eruption.** During the study period (1981–98), two large volcanic events dramatically affected the surface temperatures. The first occurred at El Chichon of Mexico in April 1982, and the second was at Mt. Pinatubo in June 1991 in the Philippines.

Volcanic sulfate aerosols change the atmosphere–surface radiation balance in the following three ways:

by scattering light in the visible wavelength, by reflecting and absorbing in the near-infrared wavelengths, and by emitting thermal longwave radiation (Andersen et al. 2001). Therefore, aerosol complicates atmospheric conditions and causes extra uncertainty in the AVHRR LST retrieval.

It is beyond our capability to accurately correct the volcanic aerosol effects because of a lack of adequate aerosol observations. Instead, we must remove the pixels that were most likely contaminated by volcanic aerosol, which are recognized by large variations on the leaf area index (LAI) field. LAI data from the AVHRR for 1981–98 are provided by the Boston University land cover group (Myneni et al. 1997). Figure 3 shows the LAI of July for 1991 and 1990. July 1991 was soon after the eruption of Mt. Pinatubo, while July 1990 is considered a normal year. The differences observed in the LAI field between these 2 yr over low latitudes (Fig. 3c) are most likely due to the aerosol eruption; such large variations are far above the averaged interannual LAI changes for these regions.

**View angle.** View angle is another possible uncertainty source for LST retrieval. A difference of 10°C can be found in LST retrieval depending on the different view angles (Minnis and Khaiyer 2000; Loeb et al. 2003). The effect is most serious when the combination of surface slope and instrument scan angle results in a local view angle greater than 60°. However, the view-angle effect may be ignored when the angle is less than 45° (Wan and Li 1997). Similarly, when averaged over several pixels, the view-angle effect is also reduced (Y. H. Kerr 2002; personal communication). As discussed above, emissivity may also vary with the viewing angle (Dozier and Warren 1982; Labeled and Stoll 1991; Rees and James 1992). Currently, no acceptable method exists to accurately correct the view-angle effect. Our quality control technique for comparing the change of 2-m  $T_a$  with that of LST can, to some degree, remove bad pixels severely affected by view-angle effect.

All of the above-discussed uncertainty sources are not independent; for example, cloud contamination correction needs the typical pattern technique. Therefore, we cannot assess the final uncertainty of LSTD by simply statistically adding up all the above uncertainties. Instead, we shall assess the LSTD uncertainty by comparing it with other independent, reliable, and resolution-comparable datasets.

**DATA.** An 18-yr (1981–98) LST diurnal cycle dataset was developed from AVHRR. The dataset gives 8-km, monthly average maximum and mini-

## Mt. Pinatubo effects on LAI

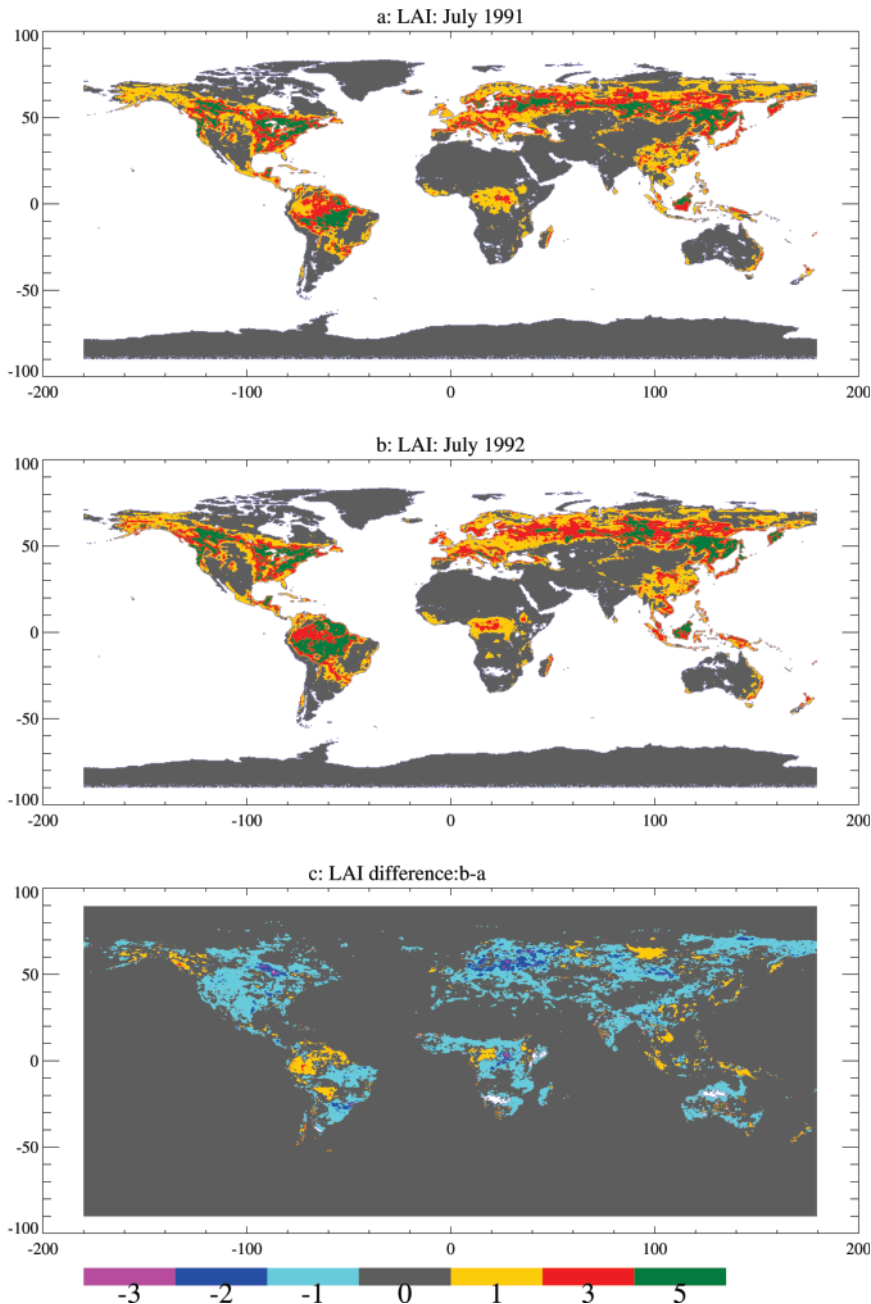


**FIG. 3.** Monthly mean AVHRR-based LAI for (a) Jul 1991, (b) Jul 1992, and (c) the difference between (a) and (b). See the text for details.

mum skin temperatures for global snow-free land surfaces.

The afternoon surface LST is obtained from the NOAA–National Aeronautics and Space Administration (NASA) Pathfinder AVHRR Land Dataset (PAL), archived at the NASA Distributed Active Archive Center (DAAC; Agbu and James 1994). The AVHRR Land Science Working Group, consisting of university and federal agency scientists, devel-

oped the Pathfinder data. The input pixels for data processing was 102,200 from AVHRR global area coverage (GAC) 1b orbital data from the NOAA polar-orbiting satellites with afternoon ascending-node equator-crossing times. The total volume of the 10-day composite dataset is 164 gigabytes, which is archived at the NASA DAAC and Products and Services Cooperative (PSC) facility. The Pathfinder AVHRR land 10-day composite dataset was derived from the daily measurement. The composition process removes much of the contamination due to cloud cover present in the daily dataset. To generate the 10-day composite dataset, 8–11 consecutive days of data are combined. The pixel with the highest Normalized Difference Vegetation Index (NDVI) for the 10 days was chosen as the date for inclusion in the composite. Choosing the highest NDVI pixel also eliminated most pixels with clouds and atmospheric contaminants. Only data within 42° of nadir were used in the composite to minimize spatial distortion and bidirectional effect biases at the edge of a scan (R. Rank 2001, personal communication). Eighteen years (1981–98) of monthly, 8-km global data, including channel-1 reflectance, channel-4 and channel-5 brightness temperatures, solar zenith angle, and land mask were obtained from this dataset. The corresponding land cover dataset was developed by the land use group at University of Maryland (DeFries et al. 1998). In addition, a lookup table of NCAR CCM3 BATS-based LST diurnal cycles was used to provide typical patterns of the LST diurnal cycle for different

land cover, seasons, and latitudes (Jin and Dickinson 1999).

The in situ surface air temperatures at half-degree resolutions from 1981 to 1998 (Jones et al. 1999; New et al. 1999) were utilized in LSTD development and validation. Surface air temperature was measured at WMO water-permeable meteorological shelters. Although this dataset has long-duration records over land areas, its sparse coverage and site relocations caused uncertainties in the  $T_a$  data (Karl et al. 1994).

We have compared LSTD with the National Centers for Environmental Prediction (NCEP)–NCAR 50-yr reanalysis (Kistler et al. 2001). The monthly averaged model output has a resolution of  $2.5^\circ \times 2.5^\circ$ . The NCEP–NCAR reanalysis, like any other GCM output, has uncertainties, but the overall geographical distribution proved to be realistic, and, therefore, suitable to evaluate LSTD.

**RESULTS AND DISCUSSIONS.** The current LSTD dataset provides monthly diurnal-averaged skin temperature, monthly maximum skin temperature ( $T_{\max}$ ), and monthly minimum skin temperature ( $T_{\min}$ ), from 1981 to 1998 at 8-km resolution. The dataset is scaled up to  $0.5^\circ \times 0.5^\circ$  and  $5^\circ \times 5^\circ$ , and is comparable to other surface temperature datasets. LSTD can be used to study the climatology of land skin temperature and its diurnal, seasonal, and interannual variations on both global and regional scales. Snow screening is done through AVHRR channel-1 and channel-2 albedo information. In the NASA DAAC AVHRR pathfinder dataset, there is a cloud mask. For cloud-free data, high channel-1 and -2 albedo information suggests the snow presence.

In this section, we present some prototype results to prove the potential values of LSTD. Meanwhile, validation of LSTD was also presented by comparing AVHRR LSTD with the surface air temperature, NCEP–NCAR reanalysis, and TOVS results.

**Climatology.** Figure 4 is the climatology of LST based on the average of January and July monthly means. These data were averaged from 1981 to 1998 at a  $5^\circ$  resolution, which was scaled up from the original 8 km. The snow-covered areas, such as polarward of  $60^\circ\text{N}$ , were not retrieved. January and July generally have the minimum and maximum temperatures in

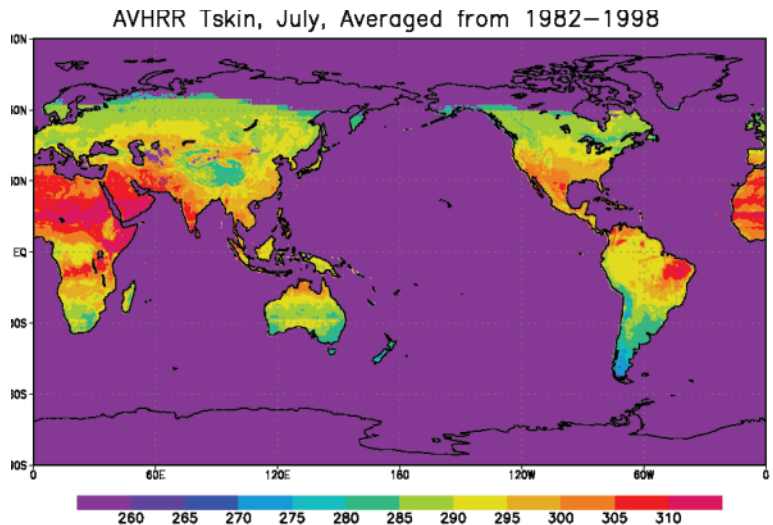
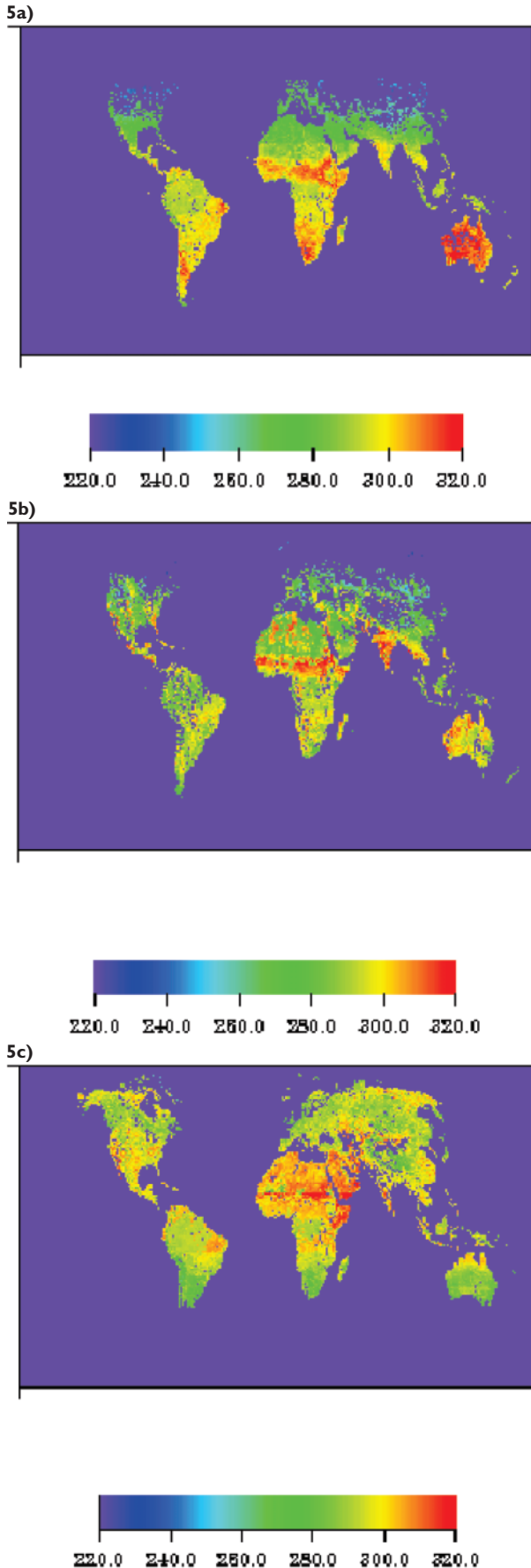


**FIG. 4.** The AVHRR-observed climatology of diurnal-averaged LST for July. Here the data are averaged from 1982 to 1998 observations. “Tskin” stands for LST.

the annual cycle; therefore, an average of these two represent the signal of the annual average. The global geographical distribution of skin temperature depends on latitude and underlying surface cover. The maximum temperatures occur at the tropical desert areas, with values up to 320 K for the Sahara. Temperature decreases from the tropical to polar regions. These features agree well with those previously observed by the high-resolution infrared sounder (HIRS; Jin et al. 1997) and are also consistent with the NCEP–NCAR reanalysis (not shown). More importantly, finer-resolution LSTD data can present spatial structures of temperature with details that are valuable for studying regional climate.

**Seasonal variation.** Figures 5a–5b show the global geographical distribution of skin temperature at 8-km resolution in January, April, and July 1988, respectively. The seasonality is evident by the extremely large values in the Northern Hemisphere desert areas in July, and in the Southern Hemisphere in January. In winter, most of the land areas in the Northern Hemisphere’s mid- to high latitudes are covered by snow and, therefore, yield no data. The total number of nonocean pixels over the globe exceeds 2,000,000, of which 90% are snow-free land for July, and only 65% for January. Therefore, we only study snow-free land areas (hereafter referred to as land).

If averaged over the same regions, which are snow-free in January, the monthly mean of LST is 300.48 K for January, 301.89 K for April, and 303.10 K for July. Compared with the global annual mean surface air temperature of 285.5 K (Sellers



1965), this obviously larger global mean skin temperature is partly due to the fact that we do not consider snow- and ocean-covered areas and the physical differences between skin and air temperatures. In addition, the global mean uses a 10-day composite of satellite observations of LST, which tends to select clear pixels for one location and, thus, underestimates cloudy days. This causes the overall LST to be a bit higher than it should. It would be more accurate to analyze the difference, anomalies, and patterns of LST rather than the absolute values. April values are limited to mid- and low latitudes. In July, high latitudes and most areas of the Tibetan Plateau are included in the global average; but, temperatures over most of those areas are relatively low, such as 275 K in Tibet. Another reason is that Southern Hemisphere land areas in July have lower temperatures than in April. Data are missing over some African equatorial areas because the high surface temperature exceeded the satellite saturation threshold and these pixels are treated as missing data in skin temperature retrieval procedure.

One advantage of global LSTD is that it spatially samples more areas than the network of WMO stations (National Research Council 2000) and may reduce any errors for regions sparsely sampled by WMO shelters. Another advantage of LSTD is that its uniformly high resolution makes it easier to study regional climate. Considerable detail of LST is presented, with 8 km per pixel resolution, which is particularly valuable for mountains or deserts. For example, by identifying the snow-covered and snow-free pixels, one could detect the extension of snow coverage and its variations over Tibet from satellite observations, which is difficult to obtain otherwise.

*Diurnal variation.* The diurnal range ( $T_{\max} - T_{\min}$ ) presented in Fig. 6 is for July 1988. The largest diurnal variation is 35°C, which was found at tropical and subtropical desert areas. The decrease of the diurnal range toward the pole is evident, but there are large diurnal variations in the central and east Siberian Plateau polarward of 60°N, as well as in land areas around Hudson Bay in North America. Artificial straight lines appear along the latitudes of 30°, 20°, 10°S, etc., which are most likely caused by the lack of AVHRR nighttime observations. (Our algorithm needs twice-per-day measurements to derive a diurnal cycle but, in this

**FIG. 5.** Seasonal variations of the diurnal-averaged monthly mean LST (K). LST is from LSTD based on AVHRR observations, as described in the text: (a) Jan 1988, (b) Apr 1988, and (c) Jul 1988, respectively.



work, the AVHRR nighttime observations are unreliable. As such, only daytime measurements are used.) However, because nighttime skin temperature varies relatively less than in daytime, and is similar to that of air temperature (Jin et al. 1997), air temperature is used whenever available to reduce the uncertainty. The artificial lines can be removed after averaging around the surrounding pixels. But, at this stage of dataset development, we prefer to leave it rather than applying a smoothing technique that would reduce the resolution of the dataset.

Further analysis shows that the diurnal change is closely related to local vegetation cover, which is consistent with other studies (Jin et al. 1997; Jin and Treadon 2003).

*Interannual variability.* A long record of global LST is highly desired for climate change studies. As a recent NRC study reported, analyses of surface air temperatures over the globe have shown a 0.2°C per decade increase in the past two decades. However, satellite observations have shown little or no increase for this period in the free atmosphere (National Research Council 2000). Because surface air temperature is observed by WMO stations, which are not uniformly sited, can the warming detected from such observations be reliable? Can it be detected from satellite surface data? These questions need to be addressed before we can better understand global warming and have the ability to predict climate change.

As a prototype for LSTD application, we examined annual global anomalies of LST changes during 1981–98 from the AVHRR LST, from 2-m surface air temperature, and from NCEP–NCAR reanalysis (Fig. 7, also see Jin and Dickinson 2002, their Fig. 1). Obviously, all three independent datasets show an increase of temperature at the surface. The rates based on LSTD, in situ data, and the NCEP–NCAR reanalysis are 0.43°C per decade, 0.34°C per decade, and 0.28°C per decade, respectively. The different increases may be due to the differences between skin and air temperatures, or may be due to different averaging methods (National Research Council 2000). However, most importantly, the consistency in the increasing trend among these independent datasets supports the surface warming theory.

AVHRR Monthly Mean Diurnal Range of  $T_s$  ( $T_{max} - T_{min}$ ), July 1988

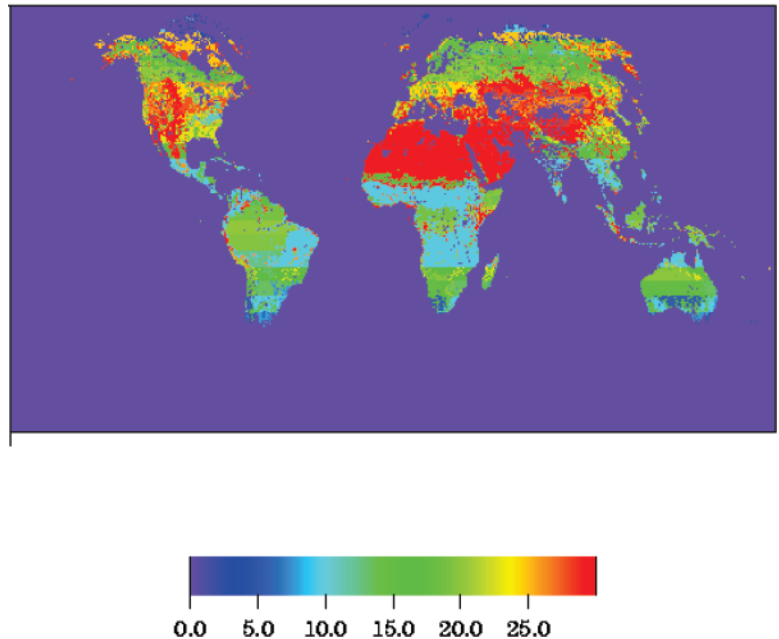


Fig. 6. The monthly mean diurnal range based on LSTD maximum and minimum skin temperatures, respectively. “ $T_{max}$ ” and “ $T_{min}$ ” stand for the maximum and minimum skin temperatures. The unit is Kelvin. Diurnal range is calculated as  $T_{max}$  minus  $T_{min}$ .

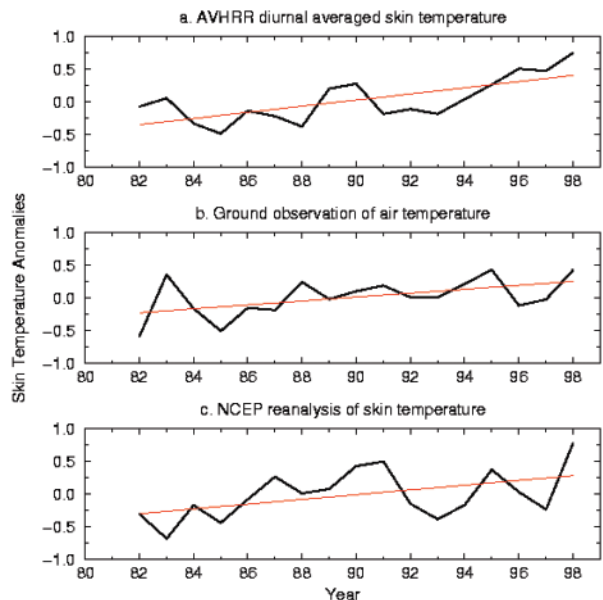


Fig. 7. Interannual variations of global monthly mean skin temperature from 1982 to 1998: (a) AVHRR LST, (b) in situ  $T_a$ , and (c) NCEP–NCAR reanalysis of LST. Data are the average of Jan and Jul. The straight line in each panel is a linear regression.

A close comparison of  $T_s$  and  $T_a$  in Fig. 7 suggests that the changes of  $T_s$  and  $T_a$  are not always the same

phase. This is partly due to the physical differences between these two variables. As Manabe and Stouffer (1996) stated, “because of the small effective thermal inertia of the continental surface, the power spectra of both land surface (LST) temperature and SAT (surface air temperature,  $T_a$ ) is almost white except at very short timescales.” Studying the differences between skin and air temperatures has been a highly desired research topic (K. E. Trenberth 2002, personal communication), partly due to the uncertainties of AVHRR data.

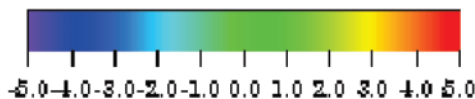
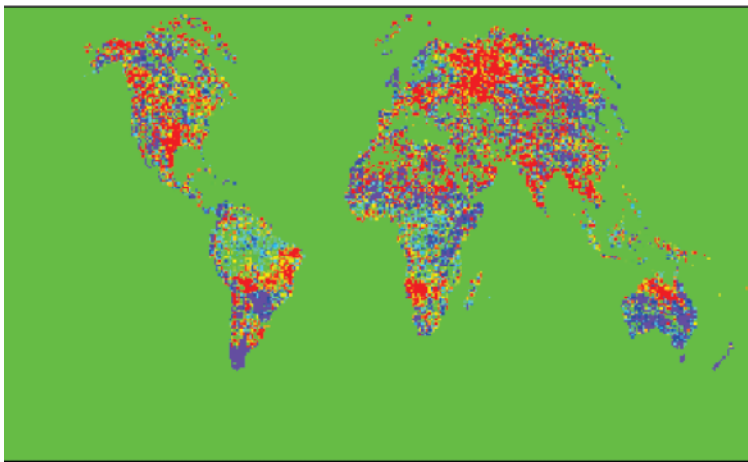
LSTD is for snow-free regions, while  $T_a$  and the NCEP–NCAR reanalysis include snow-covered land

areas. This might be another reason for the differences among the trends of the three datasets. Snow coverage varies annually and for a given area. However, statistical analyses shows that total snow-free land pixels for one latitude did not change much during these years, suggesting that for local and regional scales, snow variations are quite large, but for the global mean the impact may be reduced.

*El Niño event.* Extreme climate events, such as El Niño, dramatically change the surface temperature by displacing atmospheric circulation systems and by teleconnection. Examining whether LSTD can capture these changes, on one hand, can validate orbit drift correction. On the other hand, it can build some confidence in using LSTD to illustrate the high heterogeneities of land surface temperature. Here we compare the LSTD with the NCEP–NCAR reanalysis. LSTD data are a diurnally averaged monthly mean, which is comparable with NCEP–NCAR model simulations. Figure 8 shows the difference of 1998 and 1997 July skin temperature. July 1998 is the transition time from severe El Niño to La Niña events. Large positive changes were observed in various land surfaces, including central Eurasia, the southeast United States, northwest North America, and the north of Australia, suggesting that these regions were warmer in 1998 than in 1997. All of these warming centers are observed on LSTD. There are dissimilar areas also. For example, although the NCEP–NCAR model has captured the cold in south Australia and warmth in north Australia, south Australia is modeled too warm compared to the observations. These inconsistencies imply that improvements are needed, probably in both LSTD and NCEP–NCAR reanalyses.

8a)

Skin Temperature Diurnal Mean, 1998-1997, July



8b)

NCEP/NCAR Ranalysis, 1998-1997, July, Tskin

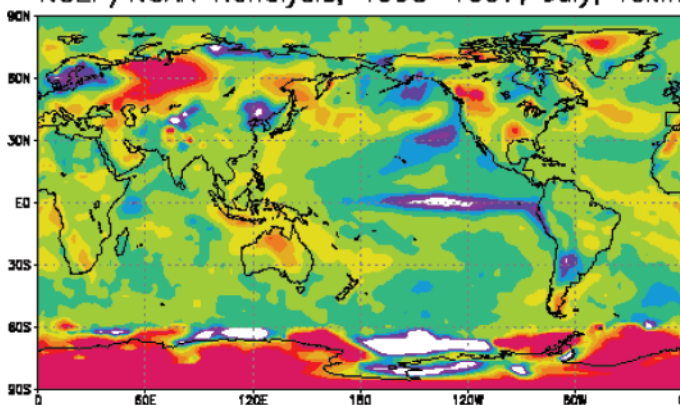


FIG. 8. Global distribution of annual variations of the diurnal-averaged LST for Jul 1998 minus 1997. “Tskin” stands for LST: (a) AVHRR and (b) NCEP–NCAR reanalysis, respectively.

**Regional variations.** Controlled by the surface energy budget, LST is determined by surface insolation. Therefore, it has obvious seasonal variations and latitude dependence, which corresponds to surface insolation. Seasonality and latitude dependencies are evident from LSTD. The zonal-mean LST anomalies during 1981–98 (Fig. 9) show that low latitudes may have larger LST variations than high latitudes, with anomalies ranging from  $+2^{\circ}$  to  $-5^{\circ}\text{C}$  for  $0^{\circ}$ – $20^{\circ}\text{N}$ , and only  $+2^{\circ}$  to  $-2^{\circ}\text{C}$  for  $60^{\circ}$ – $80^{\circ}\text{N}$ . Of course, the volcanic effect may enhance the natural variation signal at low latitudes. In addition, in July the variations of LST are not as significant as in January (not shown). These results are consistent with those from the GCM, once described in Schneider and Dickinson (1974) as a positive lapse rate feedback.

Land–biosphere–atmosphere interactions are responsible for regional climate changes. High-resolution satellite data can illustrate the land cover impacts on LST. Figure 10 shows LST anomalies over desert and semidesert areas at low latitudes. Although the trend may not be statistically significant, desert areas show larger interannual variations than those of other land cover areas. Furthermore, the diurnal range of skin temperature decreases during 1982–98 (Fig. 10b), which is similar to the globally averaged diurnal range (Jin and Dickinson 2000, their Fig. 2b).

**Further validation.** Validation is extremely important for a new dataset such as LSTD. It is also a difficult task because there is no global, in situ ground truth data available for LSTD validation. Nevertheless, comparing LSTD with other satellite observations and GCM simulations shall shed light on the data quality. We have examined LSTD using the TOVS skin temperature observations, WMO surface air temperature, and NCEP–NCAR reanalysis, as previously presented. In addition, Fig. 11 compares the zonal average of AVHRR LSTD and NCEP–NCAR LST for July 1985 and 1988, respectively. Presenting these two years is partly to examine the corrections of orbit drift, because 1985 is the beginning of the lifetime of NOAA-9, and 1988 is the transaction time of NOAA-9 and -11. Obviously, Fig. 11 shows that over most land areas, the zonal mean of LST between AVHRR and NCEP–NCAR coincide, except over tropical areas. Such a discrepancy is at least partly due to the problematic simulation of NCEP–NCAR over tropical areas (Trenberth et al. 2001).

Corresponding TOVS LST is used to validate the monthly, seasonal, and interannual variations of LST. Comparing TOVS LST with AVHRR LST shows overall agreement between the two datasets (Fig. 12).

## Zonal Mean Tskin Variations

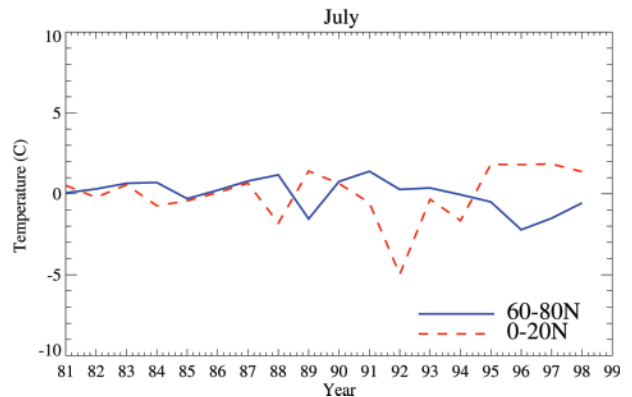


**FIG. 9.** Comparison of the zonal-mean LST anomalies during 1981–98, for  $0^{\circ}$ – $20^{\circ}\text{N}$  and  $60^{\circ}$ – $80^{\circ}\text{N}$  respectively. LST is the diurnal-averaged monthly mean from AVHRR-based observations.

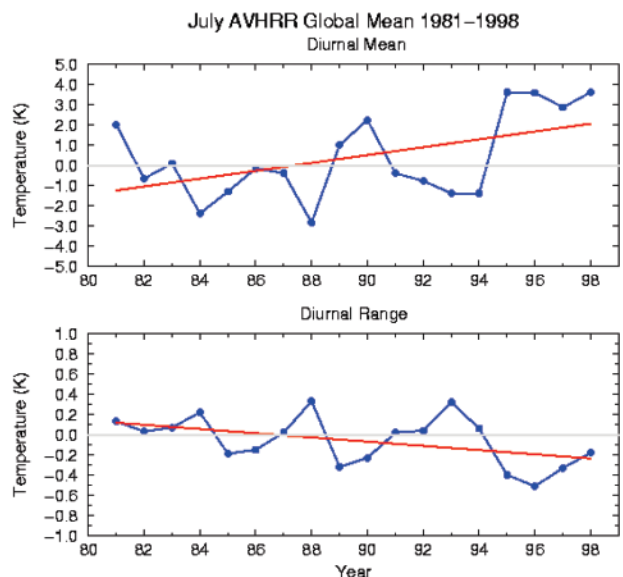


**FIG. 10.** LST anomalies over desert and semidesert areas at low latitudes. Data are from AVHRR-based LSTD: (a) diurnal-averaged monthly mean observations and (b) diurnal range of LST, namely, monthly maximum LST minus monthly minimum LST.

Both AVHRR and TOVS have extreme values of LST in tropical desert areas and the southwest United States. The minimum values are observed over the Tibetan Plateau, with TOVS values as low as 260–270 K.

**CONCLUDING REMARKS.** A long-term skin temperature diurnal cycle dataset was developed from AVHRR observations. This dataset covers global snow-free land areas and spans from 1981 to 1998. As presented, this 18-yr dataset can be used to estimate the changes of skin temperature, to study interactions

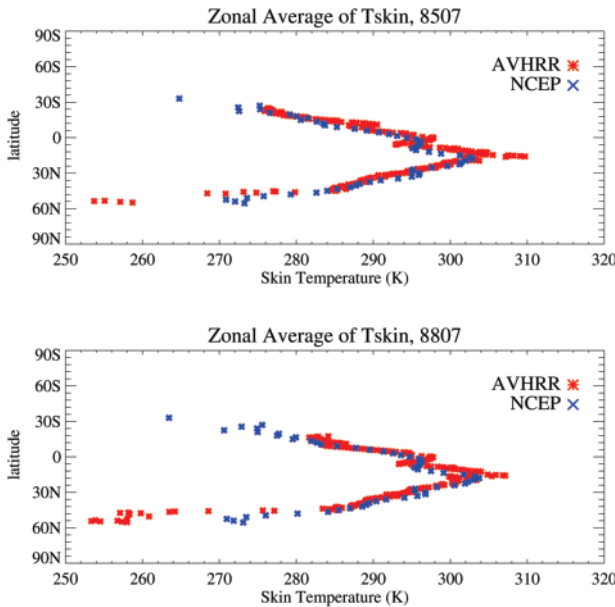


**FIG. 11. Comparison of zonal mean AVHRR-based LST with NCEP-NCAR reanalysis for (top) Jul 1985 and (bottom) Jul 1988 for land areas only.**

in the land-biosphere-atmosphere system, and to evaluate model simulations.

The value of LSTD depends on its accuracy, duration, and the possibility of applying this dataset to climate studies. Validating LSTD is an ongoing task in which LSTD is compared with other LST observations. However, Hall et al. (1992) reported difficulty in applying the skin temperature from fine-resolution satellite observations to field observations. A several degree difference was reported due to scaling and retrieval problems. Alternatively, as proven in many other cases, using LSTD in climate studies and comparing the results with existing understanding is also a practical approach to validate the dataset.

The LSTD is valuable for model development. Perhaps the most sensible approach would be to use satellite skin temperatures for model validation by directly comparing modeled and observed skin temperatures as demonstrated in Jin et al. (1997). The insights gained into physical processes could consequently improve the corresponding model parameterization scheme (Crosson et al. 1993; Smith et al. 1993).

Unlike  $T_a$ , which has been frequently used to compare with observations, the NCEP-NCAR LST has not been adequately validated over land and, thus, should not be assumed as good enough to validate other models' LST. In fact, the NCEP-NCAR LST is a diagnostic variable that is determined by the land surface model's surface ground and leaf temperatures. The latter two need to be validated. LSTD is

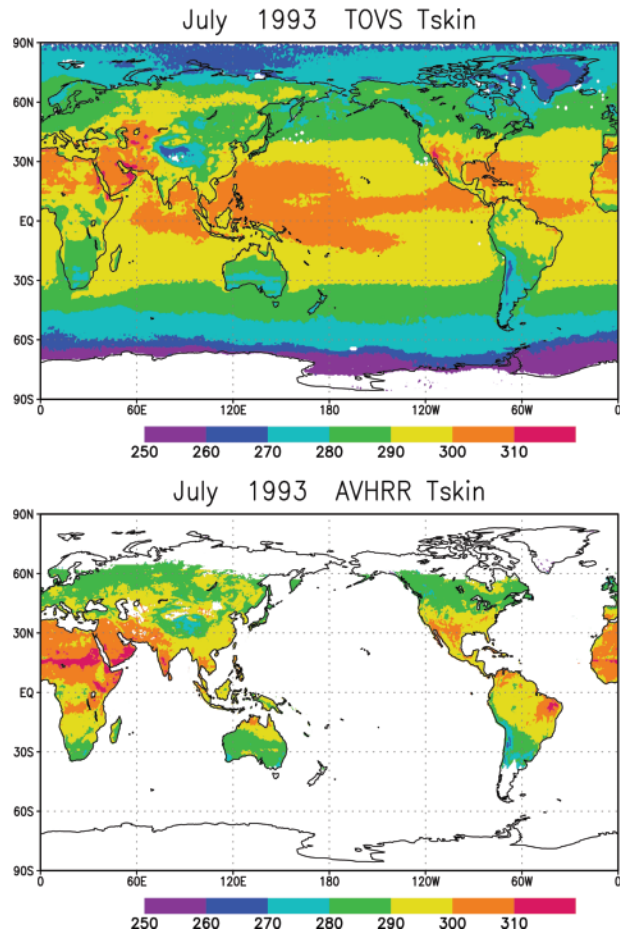


**FIG. 12. Comparison of (a) TOVS skin temperature with (b) AVHRR-based LSTD diurnal-averaged LST. Both AVHRR and TOVS data are the monthly mean for Jul 1993. The resolution of AVHRR LSTD data is  $0.5^\circ \times 0.5^\circ$  and TOVS data is  $1^\circ \times 1^\circ$ . We purposely keep the ocean LST information to show the strength of TOVS data, that is, it covers high latitudes and ocean surface.**

better than the NCEP-NCAR reanalysis in terms of both spatial resolution (8 km and up) and more information of geographical distribution.

As a prototype of LSTD application, we examined annual global anomalies of LST changes during 1981-98 from LSTD, from 2-m surface air temperature, and from the NCEP-NCAR reanalysis (Fig. 6). Obviously, all three independent datasets show an increase trend of temperature at the surface. The rates based on LSTD, in situ data, and the NCEP-NCAR reanalysis are  $0.43^\circ\text{C}$  per decade,  $0.34^\circ\text{C}$  per decade, and  $0.28^\circ\text{C}$  per decade, respectively. The consistency among these independent datasets is encouraging with regard of the quality of LSTD.

The LSTD is not meant to replace other existing datasets. Rather, it can serve as an independent, unique, and supplementary resource for climate

change studies. These long-term observations can be used to study ENSO impacts on land surface or vegetation–atmosphere–land surface interactions. For example, Jin and Zhang (2002) projected LAI anomalies on Niño-3 and showed the large correlation between LAI and El Niño over North America high latitudes. Meanwhile, calculating the correlation of LAI and skin temperature anomalies help illustrate the local vegetation–land cover impacts on skin temperature variations.

The accuracy of LSTD is related to its temporal and spatial resolutions. Based on our analyses, a less than 0.2 K per decade uncertainty is found for interannual, global anomalies (trend, Fig. 7; and see Jin and Dickinson 2002 for statistical analysis), less than half a degree for the monthly zonal mean for most regions, except over tropical areas (Fig. 11), and less than 1 K for the model grid, monthly mean for most areas (Figs. 8 and 12). The uncertainty can be up to 5 K for some tropical areas such as east of South America and the mountain areas of Tibet (Fig. 12). More importantly, we recommend that LSTD is more suitable for climate study than for research on a daily pixel level, and the differences of LSTD, instead of the absolute values, should be used to study patterns and diurnal, seasonal, and interannual variations.

**ACKNOWLEDGEMENTS.** This work is funded by the NASA EOSIDS program under Contract NAG5-10209 (Principal Investigator- Robert E. Dickinson). We thank Ms. Rebecca Ross for her help on editing the manuscript. We also thank Robert Rank for providing us with AVHRR solar zenith angle data. The dataset presented in this work can be obtained from the Department of Meteorology, University of Maryland, College Park (available online at .meto.umd.edu, or contact mjin@atmos.umd.edu).

## REFERENCES

- Agbu, P. A., and M. E. James, 1994: The NOAA/NASA Pathfinder AVHRR land data set user's manual. Goddard Distributed Active Archive Center, NASA Goddard Space Flight Center, 104 pp.
- Andersen, U. J., E. Kaas, and P. Alpert, 2001: Using analysis increments to estimate atmospheric heating rates following volcanic eruptions. *Geophys. Res. Lett.*, **28**, 991–994.
- Bates, J. J., and H. F. Diaz, 1991: Evaluation of multi-channel sea surface temperature product quality for climate monitoring: 1982–1988. *J. Geophys. Res.*, **96**, 20 613–20 622.
- Becker, F., and Z.-L. Li, 1990: Towards a local split window method over land surface. *Int. J. Remote Sens.*, **3**, 17–33.
- , and —, 1995: Surface temperature and emissivity at various scales: Definition, measurement and related problems. *Remote Sens. Rev.*, **12**, 225–253.
- Cooper, D. I., and G. Asrar, 1989: Evaluating atmospheric correction models for retrieving surface temperatures from the AVHRR over a tall grass prairie. *Remote Sens. Environ.*, **27**, 93–102.
- Crosson, W. L., E. A. Smith, and H. J. Cooper, 1993: Estimation of surface heat and moisture fluxes over a prairie grassland. 4. Impact of satellite remote sensing of slow canopy variables on performance of a hybrid biosphere model. *J. Geophys. Res.*, **98**, 4979–4999.
- DeFries, R. S., M. Hansen, J. R. G. Townshend, and R. Sohlberg, 1998: Global land cover classifications at 8 km spatial resolution: The use of training data derived from Landsat imagery in decision tree classifiers. *Int. J. Remote Sens.*, **19**, 3141–3168.
- Dickinson, R. E., 1994: Satellite systems and models for future climate change. *Future Climates of the World: A Modelling Perspective*, A. Henderson-Sellers, Ed., Vol. 16, *World Survey of Climatology*, Elsevier, 27.
- Dozier, J., and S. G. Warren, 1982: Effect of viewing angle on the infrared brightness temperature of snow. *Water Resour. Res.*, **18**, 1424–1434.
- Hall, F. G., K. F. Huemmrich, S. J. Goetz, P. J. Sellers, and J. E. Nickeson, 1992: Satellite remote sensing of surface energy balance: Success, failures, and unresolved issues in FIFE. *J. Geophys. Res.*, **97** (D17), 19 061–19 089.
- Houghton, J. T., Y. Ding, D. J. Griggs, M. Noguer, P. J. van der Linden, and D. Xiaosu, Eds., 2001: *Climate Change 2001: The Scientific Basis*. Cambridge University Press, 944 pp.
- Hurrell, J. W., and K. E. Trenberth, 1992: An evaluation of monthly mean MSU and ECMWF global atmospheric temperature for monitoring climate. *J. Climate*, **5**, 1424–1440.
- Ignatov, A., and G. Gutman, 1999: Monthly mean diurnal cycles in surface temperatures over land for global climate. *J. Climate*, **12**, 1900–1910.
- Jin, M., 2000: Interpolation of surface radiation temperature measured from polar orbiting satellites to a diurnal cycle. Part 2: Cloudy-pixel treatment. *J. Geophys. Res.*, **105**, 4061–4071.
- , and R. E. Dickinson, 1999: Interpolation of surface radiation temperature measured from polar orbiting satellites to a diurnal cycle. Part 1: Without clouds. *J. Geophys. Res.*, **104**, 2105–2116.
- , and —, 2000: A generalized algorithm for retrieving cloudy sky skin temperature from satellite thermal infrared radiances. *J. Geophys. Res.*, **105**, 27 037–27 047.

- , and —, 2002: New observational evidence for global warming from satellite data set. *Geophys. Res. Lett.*, **29** (10), doi: 10.1029/2001GL013833.
- , and D. Zhang, 2002: Changes and interactions between skin temperature and leaf area index in summer 1981–1998. *Meteor. Atmos. Phys.*, **80**, 117–129.
- , and S. Liang, 2003: Improve land surface emissivity parameter for land surface model using global remote sensing observations. *J. Climate*, submitted.
- , and R. E. Treadon, 2003: Correcting the orbit drift effect on AVHRR skin temperature measurements. *Int. J. Remote Sens.*, **24**, 1–16.
- , R. E. Dickinson, and A. M. Vogelmann, 1997: A comparison of CCM2–BATS skin temperature and surface-air temperature with satellite and surface observations. *J. Climate*, **10**, 1505–1524.
- Jones, P. D., M. New, D. E. Parker, S. Martin, and I. G. Rigor, 1999: Surface air temperature and its changes over the past 150 years. *Rev. Geophys.*, **37**, 173–200.
- Karl, T. R., R. W. Knight, and J. R. Christy, 1994: Global and hemispheric temperature trends: Uncertainties related to inadequate spatial sampling. *J. Climate*, **7**, 1144–1163.
- Kerr, Y. H., C. Guillou, J. P. Lagouarde, F. Nerry, and C. Oettle, 1997: LST processor. Algorithm theoretical basis document, 160 pp.
- Kistler, R., and Coauthors, 2001: The NCEP–NCAR 50-year reanalysis: Monthly means CD-ROM and documentation. *Bull. Amer. Meteor. Soc.*, **82**, 247–267.
- Labeled, J., and M. P. Stoll, 1991: Angular variation of land surface spectral emissivity in the thermal infrared: Laboratory investigation on bare soils. *Int. J. Remote Sens.*, **12**, 2299–2310.
- Loeb, N. G., N. M. Smith, S. Kato, W. F. Miller, S. K. Gupta, P. Minnis, and B. A. Wielicki, 2003: Angular distribution models for top-of-atmosphere radiative flux estimation from the Clouds and the Earth's Radiant Energy System instrument on the Tropical Rainfall Measuring Mission satellite. Part I: Methodology. *J. Appl. Meteor.*, **42**, 240–265.
- Manabe, S., and R. J. Stouffer, 1996: Low-frequency variability of surface air temperature in a 1000-year integration of a coupled atmosphere–ocean–land surface model. *J. Climate*, **9**, 376–393.
- Minnis, P., and M. M. Khaiyer, 2000: Anisotropy of land surface skin temperature derived from satellite data. *J. Appl. Meteor.*, **39**, 1117–1129.
- Myneni, R. B., R. R. Nemani, and S. W. Running, 1997: Estimation of global leaf area index and absorbed PAR using radiative transfer models. *IEEE Trans. Geosci. Remote Sens.*, **35**, 1380–1393.
- National Research Council, 2000: *Reconciling Observations of Global Temperature Change*. National Academy Press, 85 pp.
- New, M., M. Hulme, and P. Jones, 1999: Representing twentieth-century space–time climate variability. Part I: Development of a 1961–90 mean monthly terrestrial climatology. *J. Climate*, **12**, 829–856.
- Norman, J. M., and F. Becker, 1995: Terminology in thermal infrared remote sensing of nature surfaces. *Agric. For. Meteorol.*, **77**, 153–166.
- Prabhakara, C., V. G. Dalu, and V. G. Kunde, 1974: Estimation of sea surface temperature from remote sensing in the 11 and 13  $\mu\text{m}$  region. *J. Geophys. Res.*, **79**, 5039–5044.
- Prata, A. J., V. Caselles, C. Colland, J. A. Sobrino, and C. Oettle, 1995: Thermal remote sensing of land surface temperature from satellites: Current status and future prospects. *Remote Sens. Rev.*, **12**, 175–224.
- Price, J. C., 1984: Land surface temperature from measurements from the split window channels of the NOAA 7 Advanced Very High Resolution Radiometer. *J. Geophys. Res.*, **89**, 7231–7237.
- , 1991: Using spatial context in satellite data to infer regional scale evapotranspiration. *IEEE Trans. Geosci.*, **GE-28**, 940–948.
- Rees, W. G., and S. P. James, 1992: Angular variation of the infrared emissivity of ice and water surfaces. *Int. J. Remote Sens.*, **13**, 2873–2886.
- Schneider, S. H., and R. E. Dickinson, 1974: Climate modeling. *Rev. Geosci. Space Phys.*, **12**, 447–493.
- Sellers, W. D., 1965: *Physical Climatology*. The University of Chicago Press, 180 pp.
- Smith, E. A., H. J. Cooper, W. L. Crosson, and W. Heng-Yi, 1993: Estimation of surface heat and moisture fluxes over a prairie grassland. 3. Design of a hybrid physical/remote sensing biosphere model. *J. Geophys. Res.*, **98**, 4951–4978.
- Sobrino, J. A., Z.-L. Li, M. P. Stoll, and F. Becker, 1994: Improvements in the split-window technique for land surface temperature determination. *IEEE Trans. Geosci. Remote Sens.*, **32**, 243–253.
- Stephens, G. L., 1994: *Remote Sensing of the Lower Atmosphere: An Introduction*. Oxford University Press, 523 pp.
- Trenberth, K. E., D. P. Stepaniak, and J. W. Hurrell, 2001: Quality of reanalysis in the Tropics. *J. Climate*, **14**, 1499–1510.
- Ulivieri, C., M. M. Castronuovo, R. Francioni, and A. Cardillo, 1994: A split-window algorithm for estimating land surface temperature from satellites. *Adv. Space Res.*, **14**, 59–65.
- Wan, Z., and Z. Li, 1997: A physics-based algorithm for retrieving land-surface emissivity and temperature from EOS/MODIS data. *IEEE Trans. Geosci. Remote Sens.*, **35**, 980–996.